

Chiral superconductivity from parent Chern band and its non-Abelian generalization

Yan-Qi Wang,^{1,*} Zhi-Qiang Gao,^{2,3,*} and Hui Yang⁴

¹*Department of Physics and Joint Quantum Institute,
University of Maryland, College Park, Maryland 20742, USA*

²*Department of Physics, University of California, Berkeley, California 94720, USA*

³*Materials Sciences Division, Lawrence Berkeley National Laboratory, Berkeley, California 94720, USA*

⁴*William H. Miller III Department of Physics and Astronomy,
Johns Hopkins University, Baltimore, Maryland 21218, USA*

We propose a minimal model starting from a parent Chern band with quartic dispersion that can describe the spin-valley polarized electrons in rhombohedral tetra-layer graphene. The interplay between repulsive and attractive interactions on top of that parent Chern band is studied. We conduct standard self-consistent mean-field calculations, and find a rich phase diagram that consists of metal, quantum anomalous Hall crystal, chiral topological superconductor, as well as trivial gapped Bose-Einstein condensate. In particular, there exists a topological phase transition from the chiral superconductor to the Bose-Einstein condensate at zero temperature. Motivated by the recent experimental and theoretical studies of composite Fermi liquid in rhombohedral stacked multi-layer graphene, we further generalize the physical electron model to its composite fermion counterpart based on a field theory analysis. The chiral superconductor phase of the composite fermion becomes the non-Abelian Moore-Read quantum Hall phase. We argue that a chiral (pseudo-)spin liquid phase can emerge in the vicinity of this Moore-Read quantum Hall phase. Our work suggests rhombohedral multi-layer graphene as a potential platform for rich correlated topological phases.

Introduction— Topological superconductor (TSC) is one of the most attractive concepts in modern condensed matter physics. It can host non-Abelian quasiparticles, which are the potential building blocks of quantum computation [1–6]. In the past decades [7–25], experimental efforts have been made in searching for chiral topological superconductors, in which the time reversal symmetry is broken. Recent experimental and theoretical progress in graphene-based two-dimensional materials provide a new platform for unconventional superconductors and correlated insulators [26–44]. While the moiré superlattice often plays an important role in those systems [26–28, 45–65], it has been shown that the rhombohedral stacked multi-layer graphene exhibits chiral TSC and gate-tunable Chern bands in the absence of moiré pattern, where TSC and quantum anomalous Hall (QAH) insulator are observed at the same electron density [29–31, 37–39].

The intertwinement of topology and correlations in graphene-based two-dimensional materials can lead to rich physics. Motivated by this, we propose a minimal model starting from a parent Chern band with quartic dispersion found in rhombohedral tetra-layer graphene [29]. We consider the interplay between repulsive and attractive interactions among electrons. As a concrete example, we choose the Coulomb interaction as the repulsive interaction and the electron-phonon coupling as the attractive one, two of which are the most commonly discussed interactions in solids. Our self-consistent mean-field calculations show a rich phase diagram consists of metal, QAH crystal, chiral TSC, as well

as the trivial gapped Bose-Einstein condensate (BEC). In particular, we show there exists a topological phase transition between TSC and BEC phases at zero temperature. Motivated by the recent experimental and theoretical studies of composite Fermi liquid [32–37, 66], we further provide a field theory analysis that extend our investigation for physical electrons moving under the Berry curvature to composite fermions coupled to dynamical gauge fields, and argue that a chiral (pseudo-)spin liquid (CSL) phase [67–75] can emerge in the vicinity of the chiral TSC phase of the composite fermion [76], i.e., the non-Abelian Moore-Read quantum Hall phase [77]. Our work sheds light on investigating various correlated topological phases in graphene-based materials.

The model— We consider the following minimal model that captures the spin-valley polarized electrons projected to a single parent band,

$$H = H_0 + H_{\text{int}}. \quad (1)$$

Here, $H_0 = \sum_{\mathbf{k}} \epsilon(\mathbf{k}) c_{\mathbf{k}}^\dagger c_{\mathbf{k}}$ is the kinetic term, where $c_{\mathbf{k}}^\dagger$ is the creation operator of an electron with momentum \mathbf{k} in the parent band. According to the spin-valley polarization, the electron is single-flavored. In rhombohedral tetra-layer graphene, the parent band is believed to be a Chern band with quartic dispersion $\epsilon(\mathbf{k}) = \alpha |\mathbf{k}|^4$ [29], and the Brillouin zone (BZ) is chosen to be hexagonal to respect the C_3 symmetry. The electron filling is fixed to $\nu = 1$. The interaction H_{int} can be divided into the repulsive part and the attractive part. As an example, we consider the repulsive interaction from the electron-electron Coulomb interaction $H_{\text{e-e}}$ and the attractive interaction from the electron-phonon coupling $H_{\text{e-ph}}$ [78],

* These two authors contributed equally.

both of which are projected to the parent Chern band,

$$H_{e-e} = \sum_{\mathbf{k}_1 \mathbf{k}_2 \mathbf{k}_3 \mathbf{k}_4} \tilde{V}_{\mathbf{k}_1 \mathbf{k}_2 \mathbf{k}_3 \mathbf{k}_4} c_{\mathbf{k}_1}^\dagger c_{\mathbf{k}_2}^\dagger c_{\mathbf{k}_3} c_{\mathbf{k}_4}, \quad (2a)$$

$$H_{e-ph} = - \sum_{\mathbf{k}_1 \mathbf{k}_2 \mathbf{k}_3 \mathbf{k}_4} \tilde{U}_{\mathbf{k}_1 \mathbf{k}_2 \mathbf{k}_3 \mathbf{k}_4} c_{\mathbf{k}_1}^\dagger c_{\mathbf{k}_2}^\dagger c_{\mathbf{k}_3} c_{\mathbf{k}_4}, \quad (2b)$$

with $\tilde{V}_{\mathbf{k}_1 \mathbf{k}_2 \mathbf{k}_3 \mathbf{k}_4} = vV(\mathbf{k}_1 - \mathbf{k}_4)\mathcal{F}_{\mathbf{k}_1, \mathbf{k}_4}\mathcal{F}_{\mathbf{k}_2, \mathbf{k}_3}\delta_{\mathbf{k}_1 + \mathbf{k}_2 - \mathbf{k}_3 - \mathbf{k}_4}$ and $\tilde{U}_{\mathbf{k}_1 \mathbf{k}_2 \mathbf{k}_3 \mathbf{k}_4} = uU(\mathbf{k}_1 - \mathbf{k}_4)\mathcal{F}_{\mathbf{k}_1, \mathbf{k}_4}\mathcal{F}_{\mathbf{k}_2, \mathbf{k}_3}\delta_{\mathbf{k}_1 + \mathbf{k}_2 - \mathbf{k}_3 - \mathbf{k}_4}$. Here u, v are positive coupling constants that denote the interaction strengths. The electron-electron interaction is given by the gate-screened Coulomb potential $V(\mathbf{q}) = \tanh d|\mathbf{q}|/(d|\mathbf{q}|)$, while the electron-phonon interaction takes the form of $U(\mathbf{q}) = q_0^2/(|\mathbf{q}|^2 + q_0^2)$ [79]. In this work, we fix $d = 1.0/|\mathbf{K}|$ around the order of the screening length [32, 78], and $q_0 = 0.3|\mathbf{K}|$ satisfying $q_0 < |\mathbf{K}|$ [80][81], where \mathbf{K} denotes the momentum at the K -point of the hexagonal BZ. We then define a energy scale for kinetic term H_0 as $\epsilon_K = \alpha|\mathbf{K}|^4$, and evaluate (u, v) in terms of ϵ_K . The projected form factor \mathcal{F} encodes the quantum geometry of the parent band [78],

$$\mathcal{F}_{\mathbf{k}, \mathbf{k}'} = \exp \left[-\frac{\mathcal{B}_0}{4} (|\mathbf{k}' - \mathbf{k}|^2 + 2i\mathbf{k}' \times \mathbf{k}) \right]. \quad (3)$$

Here, \mathcal{B}_0 is the Berry curvature which can be taken as fixed parameter. Since the quartic parent Chern band can be approximately viewed as the lowest Landau level, in the following we take a uniform Berry curvature $\mathcal{B}_0 = 2\pi/\Omega_{\text{BZ}}$ corresponding to Chern number equal to one for the parent band, where Ω_{BZ} is the area of the first BZ.

Self-consistent calculation— The competition between H_{e-e} and H_{e-ph} motivates us to investigate the full phase diagram in terms of u and v . To see this, we conduct self-consistent mean-field calculations for the model Hamiltonian Eq. (1). We start from both particle-particle and particle-hole mean-field channels, and seek for self-consistent solutions for different (u, v) . For simplicity, we define $S(\mathbf{q}) = vV(\mathbf{q}) - uU(\mathbf{q})$, such that:

$$H_{\text{int}} = \sum_{\mathbf{k}_1 \mathbf{k}_2 \mathbf{k}_3 \mathbf{k}_4} \tilde{S}_{\mathbf{k}_1 \mathbf{k}_2 \mathbf{k}_3 \mathbf{k}_4} c_{\mathbf{k}_1}^\dagger c_{\mathbf{k}_2}^\dagger c_{\mathbf{k}_3} c_{\mathbf{k}_4}, \quad (4)$$

where $\tilde{S}_{\mathbf{k}_1 \mathbf{k}_2 \mathbf{k}_3 \mathbf{k}_4} = S(\mathbf{k}_1 - \mathbf{k}_4)\mathcal{F}_{\mathbf{k}_1, \mathbf{k}_4}\mathcal{F}_{\mathbf{k}_2, \mathbf{k}_3}\delta_{\mathbf{k}_1 + \mathbf{k}_2 - \mathbf{k}_3 - \mathbf{k}_4}$.

For the particle-particle channel, we decompose the electron momentum as $(\mathbf{k} + \mathbf{g}_i)$, where \mathbf{k} is defined in the first BZ, and \mathbf{g}_i labels the reciprocal lattice vectors under C_3 rotation. Under the Hartree-Fock approximation [78], the self-consistent mean-field interaction Hamiltonian can be divided into the Hartree term with $\mathbf{k}_1 = \mathbf{k}_4$ and $\mathbf{k}_2 = \mathbf{k}_3$,

$$H_{\text{H}} = \sum_{\mathbf{k}_1 \mathbf{k}_2} 2\tilde{S}_{\mathbf{k}_1 \mathbf{k}_2 \mathbf{k}_3 \mathbf{k}_4}^{g_1 g_2 g_3 g_4} P_{g_1 g_4}(\mathbf{k}_1) c_{\mathbf{k}_2 + \mathbf{g}_2}^\dagger c_{\mathbf{k}_2 + \mathbf{g}_3} + E_{\text{H}}, \quad (5)$$

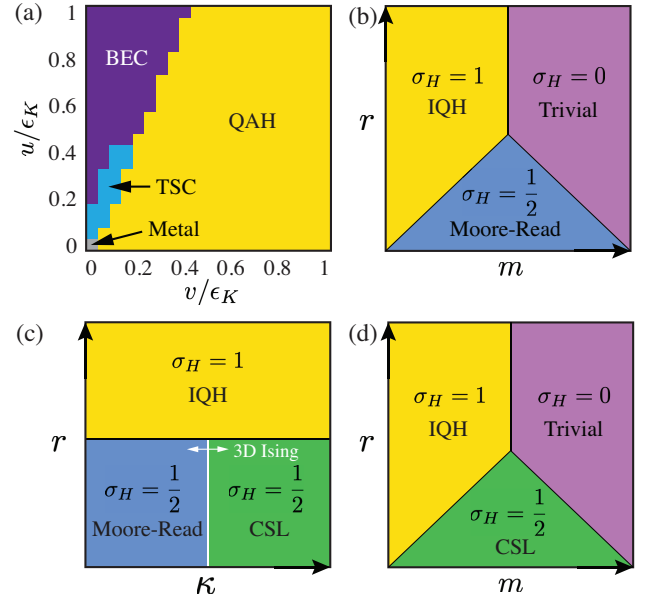


FIG. 1. (a) Phase diagram of Hamiltonian Eq. (1) from self-consistent calculations. The gray corner shows the possible metallic phase, to the accuracy of our numerics. The yellow block stands for the QAH crystal phase. The blue region denotes the $(p + ip)$ -wave TSC, and the purple block represents the trivial gapped BEC phase. (b-d) Schematic phase diagrams for the composite fermion theory Eq. (9) under fixed $\lambda, t > 0$, with (b) small Maxwell coupling κ , (c) negative composite fermion mass m , (d) large Maxwell coupling κ .

and the Fock term with $\mathbf{k}_1 = \mathbf{k}_3$ and $\mathbf{k}_2 = \mathbf{k}_4$,

$$H_{\text{F}} = - \sum_{\mathbf{k}_1 \mathbf{k}_2} 2\tilde{S}_{\mathbf{k}_1 \mathbf{k}_2 \mathbf{k}_3 \mathbf{k}_4}^{g_1 g_2 g_3 g_4} P_{g_1 g_3}(\mathbf{k}_1) c_{\mathbf{k}_2 + \mathbf{g}_2}^\dagger c_{\mathbf{k}_2 + \mathbf{g}_4} + E_{\text{F}}. \quad (6)$$

Here, E_{H} (E_{F}) is the constant energy shift from Hartree (Fock) contribution, while $\tilde{S}_{\mathbf{k}_1 \mathbf{k}_2 \mathbf{k}_3 \mathbf{k}_4}^{g_1 g_2 g_3 g_4} = S(\mathbf{k}_1 + \mathbf{g}_1 - \mathbf{k}_4 - \mathbf{g}_4)\mathcal{F}_{\mathbf{k}_1 + \mathbf{g}_1, \mathbf{k}_2 + \mathbf{g}_4}\mathcal{F}_{\mathbf{k}_2 + \mathbf{g}_2, \mathbf{k}_1 + \mathbf{g}_3}\delta_{\mathbf{g}_1 + \mathbf{g}_2 - \mathbf{g}_3 - \mathbf{g}_4}$.

For the particle-hole channel, we assume that the pairing happens between electrons with opposite momenta. In this way, the BdG Hamiltonian reads,

$$H_{\text{BdG}} = \sum_{\mathbf{k}} \Psi_{\mathbf{k}}^\dagger \begin{pmatrix} [\epsilon(\mathbf{k}) - \mu]/2 & \Delta(\mathbf{k}) \\ \Delta^*(\mathbf{k}) & [-\epsilon(\mathbf{k}) + \mu]/2 \end{pmatrix} \Psi_{\mathbf{k}}, \quad (7)$$

where $\Psi_{\mathbf{k}} = (c_{\mathbf{k}}, c_{-\mathbf{k}}^\dagger)^T$ is the Nambu spinor. Here μ is the chemical potential determined by the self-consistent equation of electron number N at filling $\nu = 1$. When $\mu < 0$, the BdG Hamiltonian Eq. 7 describes a BEC phase. The superconducting gap

$$\Delta(\mathbf{k}) = \sum_{\mathbf{k}'} \frac{1}{2} [S(\mathbf{k} - \mathbf{k}')\mathcal{F}_{\mathbf{k}, \mathbf{k}'}^2 - S(\mathbf{k} + \mathbf{k}')\mathcal{F}_{-\mathbf{k}, \mathbf{k}'}^2] \langle c_{-\mathbf{k}'} c_{\mathbf{k}'} \rangle \quad (8)$$

respects spatial asymmetry $\Delta(-\mathbf{k}) = -\Delta(\mathbf{k})$ representing the odd parity self-consistent solution of Eq. (7) for

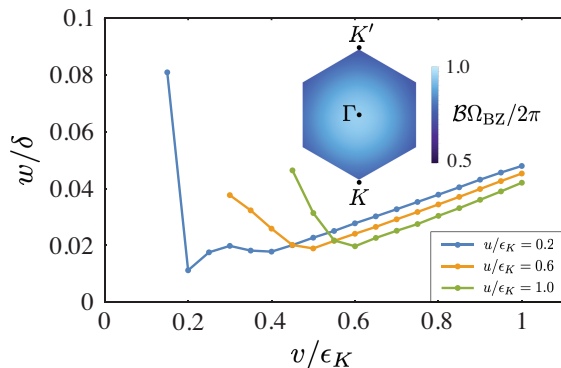


FIG. 2. The ratio between band width w and band gap δ with respect to the interacting strength u and v within the region of QAH crystal phase. The blue, orange, and green curve is plotted at $u = 0.2\epsilon_K$, $u = 0.6\epsilon_K$, and $u = 1.0\epsilon_K$, respectively. One can see that the band width w is small (less than 0.1) compared with the charge gap δ for all the (u, v) we consider. The inset shows the distribution of Berry curvature within first BZ for $u = 0$, $v = 0.2\epsilon_K$, whose integral gives Chern number $|C| = 1$.

the pairing between single-flavored electrons. We also denote $E(\mathbf{k}) = \sqrt{[\epsilon(\mathbf{k}) - \mu]^2/4 + |\Delta(\mathbf{k})|^2}$ as the dispersion of the Bogoliubov band.

Phase diagram— With above, we conduct self-consistent calculations of Eq. (1) for the particle-particle and the particle-hole channels numerically and map out the phase diagram Fig. [1.(a)] in terms of u and v varying from 0 to ϵ_K . We find that, when both u and v are small ($u, v < 0.05\epsilon_K$), the system favors a metallic phase, as shown in the gray region. A strong repulsive Coulomb interaction (i.e., large v) can drive the system to an insulating phase, with a finite charge gap δ open at the first BZ edge, as shown in the yellow region. Within the yellow region, the valence band of H_{HF} has non-trivial Chern number and order parameter $P_{g_1g_2}(\mathbf{k})$, indicating a QAH crystal phase. Note that, deep in the QAH crystal region, the band is relative flat and the distribution of Berry curvature is rather homogeneous within the first BZ, as shown in the Fig. [2]. We conjecture that the valence band is very close to the lowest Landau level which can give rise to fractional Chern insulators in the presence of moiré potential at fractional ν [32–36, 55, 56].

For the (u, v) in the blue region of Fig. [1.(a)], one can find energetic favored convergent solutions for BdG Hamiltonian Eq. (7). The superconducting gap distribution within the first BZ is shown in Fig. [3], whose real (imaginary) part has the profile of p_x -wave (p_y -wave) pairing, indicating a chiral TSC phase with $(p + ip)$ -wave pairing symmetry [5][82]. The physical origin for the chiral TSC can be understood as following. For a trivial parent band, due to the Cooper instability, a finite electron-phonon coupling will lead to s -wave superconducting phase. For a parent Chern band, the non-trivial Berry curvature will give rise to p -wave super-

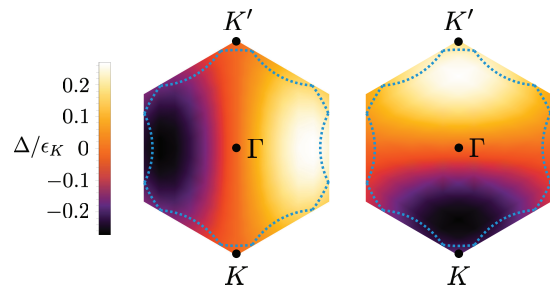


FIG. 3. Superconducting gap distribution within the first BZ with $u = 0.1\epsilon_K$, $v = 0.05\epsilon_K$. The dashed line denotes the fermi surface at $\nu = 1$. The left and right panel denotes, respectively, the real and imaginary part of $\Delta(\mathbf{k})$, which clearly shows the feature of a $(p + ip)$ -wave superconductor.

conducting phase. This is in accordance with previous work [80, 83, 84]. The vortices in bulk of this phase can trap non-Abelian Majorana zero modes [5].

In the purple region of Fig. [1.(a)] we have $\mu < 0$ that stands for the BEC phase. The transition between TSC and BEC phases here is rather interesting. The TSC phase has positive chemical potential μ . Deep in the TSC phase, the electrons are dominantly paired close to the Fermi surface, in accordance with the fact that the Bogoliubov band gap is approximately minimized near the first BZ edge deep in the TSC phase. This can be checked for the inset of $u = 0.1\epsilon_K$ in Fig. [4] showing the corresponding Bogoliubov band dispersion. The Cooper pair is extended in real space. The increasing of electron-phonon interaction u leads to the drop of μ as well as the decreasing of the Cooper pair size, such that the electrons deep in the Fermi sea starts to pair. Different from the case of s -wave, for $(p + ip)$ -wave there exists a critical u^* where $\mu = 0$ and Bogoliubov band gap closes at the Γ point. This can be seen that $E(\mathbf{k} = 0) = 0$ when $\mu = 0$ and $\Delta(\mathbf{k} = 0) = 0$ for $(p + ip)$ -wave. The Chern number for the Bogoliubov band changes from 1 in TSC phase to 0 in BEC phase, signaling a topological phase transition from the TSC to the trivial gapped BEC phase. In the BEC phase, the more negative μ is, the more electrons in the Fermi sea are paired and the size of the Cooper pairs are smaller. The gap of Bogoliubov band is minimal at Γ point, as shown in the insets with $u = 0.47\epsilon_K$ and $u = 0.6\epsilon_K$ in Fig. [4]. Details of the topological phase transition from TSC to BEC phases with fixed $v = 0.05\epsilon_K$ and varying u are shown in Fig. [4]. We point out that at finite temperature such a phase transition will change to crossover [85].

Generalization to composite fermion theory— The phase diagram Fig. [1.(a)] provides insights to study the potential non-Abelian quantum Hall phase in rhombohedral multi-layer graphene, in which the composite fermi liquid has been studied both experimentally [37] and theoretically [32]. It is natural to extend our model Eq. (1) with physical electrons moving in the background

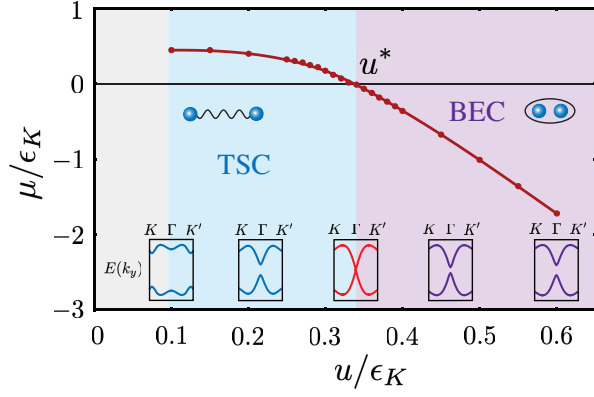


FIG. 4. Transition between the chiral TSC (blue region) and the trivial BEC phase (purple region), with $v = 0.05\epsilon_K$ and $u \in [0.1, 0.6]\epsilon_K$. One can see the chemical potential (μ) drop as the increasing of the electron-phonon coupling strength (u). The bottom insets illustrate the band structure of Bogoliubov quasiparticles. The band gap closes at the critical point ($u^* \approx 0.33\epsilon_K, \mu = 0$), indicating the topological phase transition from chiral TSC to trivial BEC phase.

Berry curvature to that of the composite fermion coupled to the dynamical gauge field. The chiral TSC phase for the composite fermion is proposed to be described by the Moore-Read [1, 77] quantum Hall state, which exhibits non-Abelian topological order. Below we generalize the phase diagram Fig. [1.(a)] into the composite fermion case with the help of field theory. The composite fermions in the presence of pairing can be modeled as [76, 86, 87]

$$\begin{aligned} \mathcal{L} = & \bar{\psi}i\gamma^\mu(\partial_\mu - ia_\mu)\psi - \frac{i}{8\pi}ada + m\bar{\psi}\psi + \frac{1}{2\kappa}(da)^2 \\ & + |D_{2a}\Phi|^2 + r|\Phi|^2 + t|\Phi|^4 - \lambda(\Phi^\dagger\psi_+\psi_- + h.c.) \\ & - \frac{i}{2\pi}adb - \frac{2i}{4\pi}bdb - \frac{i}{2\pi}bdA. \end{aligned} \quad (9)$$

Here gamma matrices can be chosen as $\gamma^0 = \sigma^z$, $\gamma^1 = i\sigma^y$, and $\gamma^2 = -i\sigma^x$ [76]. The composite fermion ψ is a two-component Dirac fermion with mass m . It is charged under the dynamical compact $U(1)$ gauge field a , and κ is the Maxwell coupling of a . The complex boson field Φ describes the pairing of the composite fermion, which is consequently charge-2 under the gauge field a . Its condensation is controlled by r , with the coupling constant of the quartic term t set to be large and positive. The λ -term ($\lambda > 0$) describes s -wave pairing for the Dirac composite fermion, which is equivalent to the chiral TSC for the non-relativistic composite fermion [76]. This is due to the intrinsic Berry curvature of the Dirac fermion, with a similar mechanism that Berry curvature can turn the s -wave superconductor into a chiral one in the physical fermion case [80, 88]. Dynamical compact $U(1)$ gauge field b is coupled to the background gauge field A through a mutual Chern-Simons (CS) term, whose flux corresponds to the current of the physical electron.

The Maxwell coupling of b is neglected since it is more irrelevant than the self CS term.

The phase diagram of Eq. (9) can be analyzed at the mean-field level. We first consider the non-superconducting phases. This corresponds to $r > 0$, where Φ is gapped and ψ can be integrated out. The resulting topological part of the Lagrangian reads

$$\mathcal{L}_{\text{QH}} = -\Theta(-m)\frac{i}{4\pi}ada - \frac{i}{2\pi}adb - \frac{2i}{4\pi}bdb - \frac{i}{2\pi}bdA. \quad (10)$$

The topological data, including ground state degeneracy, Hall conductance, anyon charge and statistics can be extracted from the standard K -matrix theory [89]. We find that the Hall conductance is $\sigma_H = 0$ or $\sigma_H = 1$ for m positive or negative, corresponding to a trivial or an integer quantum Hall (IQH) phase, respectively. Meanwhile, since the absolute value of the determinant of the K -matrix for Eq. (10) equals to one, neither of the two phases are topological ordered due to the trivial ground state degeneracy. Thus the $\sigma_H = 1$ ($\sigma_H = 0$) phase is topological equivalent to the QAH crystal (gapped BEC) phase in the phase diagram Fig. [1.(a)]. Though the gapped BEC phase exhibits superconductivity while in the $\sigma_H = 0$ phase the composite fermion does not pair, these two phases are topological equivalent as discussed in the study of proximity effect [5, 90].

When $r < 0$, Φ is condensed, driving the system into superconducting phase for the composite fermion ψ . Correspondingly, the $U(1)$ gauge field a is Higgsed to \mathbb{Z}_2 . The pairing potential ensures ψ to remain gapped regardless the sign of m , as long as $|m| < |\lambda\langle\Phi\rangle|$. Thus, integrating out ψ naively yields the effective Lagrangian

$$\mathcal{L}_{\text{MR}} = \frac{1}{2\kappa}(da)^2 + \frac{2i}{2\pi}ad\tilde{a} - \frac{i}{2\pi}adb - \frac{2i}{4\pi}bdb - \frac{i}{2\pi}bdA, \quad (11)$$

where \tilde{a} is the Lagrange multiplier introduced such that a is indeed a \mathbb{Z}_2 gauge field [91]. The Hall conductance in this phase is $\sigma_H = 1/2$, and the vortex whose current is coupled to \tilde{a} has charge $Q_v = 1/4$ and self-statistical angle $\theta_v = \pi/8$. The quasi hole coupled to gauge field b has half charge $Q_h = 1/2$ and semionic self-statistics $\theta_h = \pi/2$. These topological data exactly match those in the non-Abelian Moore-Read quantum Hall state. However, Eq. (11) only captures the Abelian part of the anyon statistics. To incorporate non-Abelian statistics, one need to include Majorana zero modes arising naturally in the chiral superconducting phase of the composite fermion. One way to include Majorana after integrating out ψ is to substitute the $\tilde{a}da$ term by $(\tilde{a} + \eta id\eta/4)da$ [92], where η describes the Majorana zero mode trapped at the superconducting vortex core. This gives rise to the desired non-Abelian statistics [92] in the Moore-Read state. The non-Abelian Moore-Read quantum Hall phase is corresponding to $(p + ip)$ -wave chiral TSC phase in Fig. [1.(a)]. It is important to note that the Pfaffian and the anti-Pfaffian quantum Hall phases

with similar non-Abelian statistics can be also achieved by tuning the pairing symmetry of the composite fermion in Eq. (9) [76].

In the composite fermion theory, there is an additional phase without a counterpart in the physical electron model and phase diagram Fig. [1.(a)]. To see this, note that when the composite fermion pairs, the gauge field a is a \mathbb{Z}_2 gauge field which can be confined by increasing the Maxwell coupling κ through a 3D Ising transition [93]. When a is confined, the topological part of the theory reads

$$\mathcal{L}_{\text{CSL}} = -\frac{2i}{4\pi}bdb - \frac{i}{2\pi}bdA = \frac{1}{2}\frac{i}{4\pi}AdA, \quad (12)$$

where in passing to the second equality the gapped gauge field b is integrated out, yielding a same Hall conductance $\sigma_H = 1/2$ as the Moore-Read phase discussed previously. This phase is a CSL phase with an Abelian semion whose current is coupled to b . Therefore, we conjecture the existence of the CSL phase in the vicinity of the Moore-Read quantum Hall phase with Hall conductance $\sigma_H = 1/2$ in multi-layer graphene systems.

Equipped with above analysis, we can map out the phase diagram of the composite fermion theory Eq. (9), as shown in Fig. [1 (b-d)]. Fig. [1.(b)] shows when Maxwell coupling κ is small, there will be three phases, IQH, Moore-Read, and trivial gapped phases. This is similar to the result in physical electron model shown in Fig. [1.(a)]. When κ is strong, the confinement of the \mathbb{Z}_2 gauge field will drive the Moore-Read phase into the CSL phase, as shown in Fig. [1.(d)]. In (b) and (d) the phase boundary between the superconducting (Moore-Read or CSL) and insulating (IQH or trivial) phase of composite fermion should be located at $m = \pm\lambda\langle\Phi\rangle$ for $r < 0$. Fig. [1.(c)] is plotted when the composite fermion mass $m < 0$, which explicitly shows the 3D Ising transition between the Moore-Read phase and the CSL phase. The phase boundary between the Moore-Read and the CSL phase can in principle depend on κ .

Discussion— In this work, we discuss the phase diagram of spin-valley polarized electrons under parent Chern band in the presence of both attractive and repulsive interactions. While our study is focused on the parent band with Chern number equals to one, it's natural to generalize this set up to the case with higher Chern numbers. We conjecture that more ways of asymmetric pairing, such as $(f + if)$ -wave and $(h + ih)$ -wave, can emerge. Our field theory analysis predicts the existence of chiral (pseudo-)spin liquid in the vicinity of the non-Abelian Moore-Read quantum Hall phase, and it will be an interesting future direction to verify it with state-of-the-art numerical methods.

Acknowledgements— We acknowledge Srinivas Raghu, Jing-Yuan Chen, and Zhaoyu Han for discussions on related topics. We also thank Joel E. Moore, Chunxiao Liu, Zhihuan Dong, Taige Wang, Yang-Zhi Chou and Jihang

Zhu for helpful discussions. Y.-Q. W. is supported by JQI postdoctoral fellowship at the University of Maryland. Z.-Q. G. is funded through the U.S. Department of Energy, Office of Science, Office of Basic Energy Sciences, Materials Sciences and Engineering Division under Contract No. DE-AC02-05-CH11231 (Theory of Materials program KC2301).

-
- [1] N. Read and D. Green, Paired states of fermions in two dimensions with breaking of parity and time-reversal symmetries and the fractional quantum hall effect, *Physical Review B* **61**, 10267 (2000).
 - [2] A. P. Schnyder, S. Ryu, A. Furusaki, and A. W. W. Ludwig, Classification of topological insulators and superconductors in three spatial dimensions, *Phys. Rev. B* **78**, 195125 (2008).
 - [3] C. Nayak, S. H. Simon, A. Stern, M. Freedman, and S. Das Sarma, Non-abelian anyons and topological quantum computation, *Reviews of Modern Physics* **80**, 1083 (2008).
 - [4] A. Kitaev, Periodic table for topological insulators and superconductors, in *AIP conference proceedings*, Vol. 1134 (American Institute of Physics, 2009) pp. 22–30.
 - [5] X.-L. Qi and S.-C. Zhang, Topological insulators and superconductors, *Rev. Mod. Phys.* **83**, 1057 (2011).
 - [6] M. Sato and Y. Ando, Topological superconductors: a review, *Reports on Progress in Physics* **80**, 076501 (2017).
 - [7] M. Sato and Y. Ando, Topological superconductors: a review, *Reports on Progress in Physics* **80**, 076501 (2017).
 - [8] Y.-T. Hsu, A. Vaezi, M. H. Fischer, and E.-A. Kim, Topological superconductivity in monolayer transition metal dichalcogenides, *Nature Communications* **8**, 14985 (2017).
 - [9] T. Le, Z. Pan, Z. Xu, J. Liu, J. Wang, Z. Lou, X. Yang, Z. Wang, Y. Yao, C. Wu, and X. Lin, Superconducting diode effect and interference patterns in kagome csv3sb5, *Nature* **630**, 64 (2024).
 - [10] J.-X. Yin, B. Lian, and M. Z. Hasan, Topological kagome magnets and superconductors, *Nature* **612**, 647 (2022).
 - [11] C. Mielke, D. Das, J. X. Yin, H. Liu, R. Gupta, Y. X. Jiang, M. Medarde, X. Wu, H. C. Lei, J. Chang, P. Dai, Q. Si, H. Miao, R. Thomale, T. Neupert, Y. Shi, R. Khasanov, M. Z. Hasan, H. Luetkens, and Z. Guguchia, Time-reversal symmetry-breaking charge order in a kagome superconductor, *Nature* **602**, 245 (2022).
 - [12] X. Xu, Y. Li, and C. L. Chien, Observation of odd-parity superconductivity with the geshkenbein-larkin-barone composite rings, *Phys. Rev. Lett.* **132**, 056001 (2024).
 - [13] Z. Wan, G. Qiu, H. Ren, Q. Qian, Y. Li, D. Xu, J. Zhou, J. Zhou, B. Zhou, L. Wang, T.-H. Yang, Z. Sofer, Y. Huang, K. L. Wang, and X. Duan, Unconventional superconductivity in chiral molecule-tas2 hybrid superlattices, *Nature* **632**, 69 (2024).
 - [14] F. Ming, X. Wu, C. Chen, K. D. Wang, P. Mai, T. A. Maier, J. Strockoz, J. W. F. Venderbos, C. González, J. Ortega, S. Johnston, and H. H. Weiering, Evidence for chiral superconductivity on a silicon surface, *Nature*

- Physics **19**, 500 (2023).
- [15] R. Nandkishore, L. S. Levitov, and A. V. Chubukov, Chiral superconductivity from repulsive interactions in doped graphene, *Nature Physics* **8**, 158 (2012).
- [16] F. Theuss, A. Shragai, G. Grissonnanche, I. M. Hayes, S. R. Saha, Y. S. Eo, A. Suarez, T. Shishidou, N. P. Butch, J. Paglione, and B. J. Ramshaw, Single-component superconductivity in ut_2 at ambient pressure, *Nature Physics* **20**, 1124 (2024).
- [17] L. Jiao, S. Howard, S. Ran, Z. Wang, J. O. Rodriguez, M. Sigrist, Z. Wang, N. P. Butch, and V. Madhavan, Chiral superconductivity in heavy-fermion metal ut_2 , *Nature* **579**, 523 (2020).
- [18] I. M. Hayes, D. S. Wei, T. Metz, J. Zhang, Y. S. Eo, S. Ran, S. R. Saha, J. Collini, N. P. Butch, D. F. Agterberg, A. Kapitulnik, and J. Paglione, Multicomponent superconducting order parameter in ut_2 , *Science* **373**, 797 (2021).
- [19] S. Ran, C. Eckberg, Q.-P. Ding, Y. Furukawa, T. Metz, S. R. Saha, I.-L. Liu, M. Zic, H. Kim, J. Paglione, and N. P. Butch, Nearly ferromagnetic spin-triplet superconductivity, *Science* **365**, 684 (2019).
- [20] N. T. Huy, A. Gasparini, D. E. de Nijs, Y. Huang, J. C. P. Klaasse, T. Gortenmulder, A. de Visser, A. Hamann, T. Görlach, and H. v. Löhneysen, Superconductivity on the border of weak itinerant ferromagnetism in $ucog_2$, *Phys. Rev. Lett.* **99**, 067006 (2007).
- [21] D. Aoki, A. Huxley, E. Ressouche, D. Braithwaite, J. Flouquet, J.-P. Brison, E. Lhotel, and C. Paulsen, Coexistence of superconductivity and ferromagnetism in $urhg_2$, *Nature* **413**, 613 (2001).
- [22] G. R. Stewart, Z. Fisk, J. O. Willis, and J. L. Smith, Possibility of coexistence of bulk superconductivity and spin fluctuations in upt_3 , *Phys. Rev. Lett.* **52**, 679 (1984).
- [23] S. S. Saxena, P. Agarwal, K. Ahilan, F. M. Grosche, R. K. W. Haselwimmer, M. J. Steiner, E. Pugh, I. R. Walker, S. R. Julian, P. Monthoux, G. G. Lonzarich, A. Huxley, I. Sheikin, D. Braithwaite, and J. Flouquet, Superconductivity on the border of itinerant-electron ferromagnetism in uge_2 , *Nature* **406**, 587 (2000).
- [24] S. Ghosh, A. Shekhter, F. Jerzembeck, N. Kikugawa, D. A. Sokolov, M. Brando, A. P. Mackenzie, C. W. Hicks, and B. J. Ramshaw, Thermodynamic evidence for a two-component superconducting order parameter in sr_2ruo_4 , *Nature Physics* **17**, 199 (2021).
- [25] Y. Maeno, H. Hashimoto, K. Yoshida, S. Nishizaki, T. Fujita, J. G. Bednorz, and F. Lichtenberg, Superconductivity in a layered perovskite without copper, *Nature* **372**, 532 (1994).
- [26] Y. Cao, V. Fatemi, S. Fang, K. Watanabe, T. Taniguchi, E. Kaxiras, and P. Jarillo-Herrero, Unconventional superconductivity in magic-angle graphene superlattices, *Nature* **556**, 43 (2018).
- [27] M. Yankowitz, S. Chen, H. Polshyn, Y. Zhang, K. Watanabe, T. Taniguchi, D. Graf, A. F. Young, and C. R. Dean, Tuning superconductivity in twisted bilayer graphene, *Science* **363**, 1059 (2019).
- [28] X. Lu, P. Stepanov, W. Yang, M. Xie, M. A. Aamir, I. Das, C. Urgell, K. Watanabe, T. Taniguchi, G. Zhang, A. Bachtold, A. H. MacDonald, and D. K. Efetov, Superconductors, orbital magnets and correlated states in magic-angle bilayer graphene, *Nature* **574**, 653 (2019).
- [29] T. Han, Z. Lu, Y. Yao, L. Shi, J. Yang, J. Seo, S. Ye, Z. Wu, M. Zhou, H. Liu, *et al.*, Signatures of chiral superconductivity in rhombohedral graphene, arXiv preprint arXiv:2408.15233 (2024).
- [30] M. Geier, M. Davydova, and L. Fu, Chiral and topological superconductivity in isospin polarized multilayer graphene (2024), arXiv:2409.13829 [cond-mat.supr-con].
- [31] J. Cai, E. Anderson, C. Wang, X. Zhang, X. Liu, W. Holtzmann, Y. Zhang, F. Fan, T. Taniguchi, K. Watanabe, Y. Ran, T. Cao, L. Fu, D. Xiao, W. Yao, and X. Xu, Signatures of fractional quantum anomalous hall states in twisted mo_2 , *Nature* **622**, 63 (2023).
- [32] B. Zhou, H. Yang, and Y.-H. Zhang, Fractional quantum anomalous hall effects in rhombohedral multilayer graphene in the moiréless limit and in coulomb imprinted superlattice, arXiv preprint arXiv:2311.04217 (2023).
- [33] Z. Dong, A. S. Patri, and T. Senthil, Theory of quantum anomalous hall phases in pentalayer rhombohedral graphene moiré structures (2024), arXiv:2311.03445 [cond-mat.str-el].
- [34] Z. Dong, A. S. Patri, and T. Senthil, Stability of anomalous hall crystals in multilayer rhombohedral graphene (2024), arXiv:2403.07873 [cond-mat.str-el].
- [35] J. Dong, T. Wang, T. Wang, T. Soejima, M. P. Zaletel, A. Vishwanath, and D. E. Parker, Anomalous hall crystals in rhombohedral multilayer graphene i: Interaction-driven chern bands and fractional quantum hall states at zero magnetic field (2024), arXiv:2311.05568 [cond-mat.str-el].
- [36] T. Soejima, J. Dong, T. Wang, T. Wang, M. P. Zaletel, A. Vishwanath, and D. E. Parker, Anomalous hall crystals in rhombohedral multilayer graphene ii: General mechanism and a minimal model (2024), arXiv:2403.05522 [cond-mat.str-el].
- [37] Z. Lu, T. Han, Y. Yao, A. P. Reddy, J. Yang, J. Seo, K. Watanabe, T. Taniguchi, L. Fu, and L. Ju, Fractional quantum anomalous hall effect in multilayer graphene, *Nature* **626**, 759 (2024).
- [38] Y.-Z. Chou, J. Zhu, and S. D. Sarma, Intravalley spin-polarized superconductivity in rhombohedral tetralayer graphene, arXiv preprint arXiv:2409.06701 (2024).
- [39] M. Kim, A. Timmel, L. Ju, and X.-G. Wen, Topological chiral superconductivity, arXiv preprint arXiv:2409.18067 (2024).
- [40] Y. Choi, Y. Choi, M. Valentini, C. L. Patterson, L. F. W. Holleis, O. I. Sheekey, H. Stoyanov, X. Cheng, T. Taniguchi, K. Watanabe, and A. F. Young, Electric field control of superconductivity and quantized anomalous hall effects in rhombohedral tetralayer graphene (2024), arXiv:2408.12584 [cond-mat.mes-hall].
- [41] S. D. Sarma and M. Xie, Thermal crossover from a chern insulator to a fractional chern insulator in pentalayer graphene (2024), arXiv:2408.10931 [cond-mat.mes-hall].
- [42] Z. Han, K.-S. Kim, S. A. Kivelson, and T. H. Hansson, Two-fluid theory of composite bosons and fermions and the quantum hall proximity effect, *Phys. Rev. B* **108**, 195117 (2023).
- [43] Z. Han, J. Herzog-Arbeitman, B. A. Bernevig, and S. A. Kivelson, “quantum geometric nesting” and solvable model flat-band systems, *Phys. Rev. X* **14**, 041004 (2024).
- [44] A. P. Reddy, N. Paul, A. Abouelkomsan, and L. Fu, Non-abelian fractionalization in topological minibands (2024), arXiv:2403.00059 [cond-mat.mes-hall].
- [45] H. Yang, Z.-Q. Gao, and F. Wang, Effects of defects in

- superconducting phase of twisted bilayer graphene, arXiv preprint arXiv:1908.09555 (2019).
- [46] G. Chen, A. L. Sharpe, P. Gallagher, I. T. Rosen, E. J. Fox, L. Jiang, B. Lyu, H. Li, K. Watanabe, T. Taniguchi, *et al.*, Signatures of tunable superconductivity in a trilayer graphene moiré superlattice, *Nature* **572**, 215 (2019).
- [47] H. Zhou, T. Xie, T. Taniguchi, K. Watanabe, and A. F. Young, Superconductivity in rhombohedral trilayer graphene, *Nature* **598**, 434 (2021).
- [48] P. A. Pantaleón, A. Jimeno-Pozo, H. Sainz-Cruz, V. T. Phong, T. Cea, and F. Guinea, Superconductivity and correlated phases in non-twisted bilayer and trilayer graphene, *Nature Reviews Physics* **5**, 304 (2023).
- [49] Y. Zhang, R. Polski, A. Thomson, É. Lantagne-Hurtubise, C. Lewandowski, H. Zhou, K. Watanabe, T. Taniguchi, J. Alicea, and S. Nadj-Perge, Enhanced superconductivity in spin-orbit proximitized bilayer graphene, *Nature* **613**, 268 (2023).
- [50] L. Holleis, C. L. Patterson, Y. Zhang, H. M. Yoo, H. Zhou, T. Taniguchi, K. Watanabe, S. Nadj-Perge, and A. F. Young, Ising superconductivity and nematicity in bernal bilayer graphene with strong spin orbit coupling, arXiv preprint arXiv:2303.00742 (2023).
- [51] C. Li, F. Xu, B. Li, J. Li, G. Li, K. Watanabe, T. Taniguchi, B. Tong, J. Shen, L. Lu, *et al.*, Tunable superconductivity in electron-and hole-doped bernal bilayer graphene, *Nature* , 1 (2024).
- [52] Y. Zhang, G. Shavit, H. Ma, Y. Han, K. Watanabe, T. Taniguchi, D. Hsieh, C. Lewandowski, F. von Oppen, Y. Oreg, *et al.*, Twist-programmable superconductivity in spin-orbit coupled bilayer graphene, arXiv preprint arXiv:2408.10335 (2024).
- [53] C. L. Patterson, O. I. Sheekey, T. B. Arp, L. F. Holleis, J. M. Koh, Y. Choi, T. Xie, S. Xu, E. Redekop, G. Babikyan, *et al.*, Superconductivity and spin canting in spin-orbit proximitized rhombohedral trilayer graphene, arXiv preprint arXiv:2408.10190 (2024).
- [54] J. Yang, X. Shi, S. Ye, C. Yoon, Z. Lu, V. Kakani, T. Han, J. Seo, L. Shi, K. Watanabe, *et al.*, Diverse impacts of spin-orbit coupling on superconductivity in rhombohedral graphene, arXiv preprint arXiv:2408.09906 (2024).
- [55] Z. Lu, T. Han, Y. Yao, J. Yang, J. Seo, L. Shi, S. Ye, K. Watanabe, T. Taniguchi, and L. Ju, Extended quantum anomalous hall states in graphene/hbn moiré superlattices (2024), arXiv:2408.10203 [cond-mat.mes-hall].
- [56] A. S. Patri, Z. Dong, and T. Senthil, Extended quantum anomalous hall effect in moiré structures: phase transitions and transport (2024), arXiv:2408.11818 [cond-mat.str-el].
- [57] L.-Q. Xia, S. C. de la Barrera, A. Uri, A. Sharpe, Y. H. Kwan, Z. Zhu, K. Watanabe, T. Taniguchi, D. Goldhaber-Gordon, L. Fu, T. Devakul, and P. Jarillo-Herrero, Helical trilayer graphene: a moiré platform for strongly-interacting topological bands (2023), arXiv:2310.12204 [cond-mat.mes-hall].
- [58] D. Waters, R. Su, E. Thompson, A. Okounkova, E. Arreguin-Martinez, M. He, K. Hinds, K. Watanabe, T. Taniguchi, X. Xu, Y.-H. Zhang, J. Folk, and M. Yankowitz, Topological flat bands in a family of multilayer graphene moiré lattices (2024), arXiv:2405.05913 [cond-mat.mes-hall].
- [59] H. Yang and Y.-H. Zhang, Exciton- and light-induced ferromagnetism from doping a moiré mott insulator, *Phys. Rev. B* **110**, L041115 (2024).
- [60] X.-Y. Song, Y.-H. Zhang, and T. Senthil, Phase transitions out of quantum hall states in moiré materials, *Phys. Rev. B* **109**, 085143 (2024).
- [61] Y. Jia, J. Yu, J. Liu, J. Herzog-Arbeitman, Z. Qi, H. Pi, N. Regnault, H. Weng, B. A. Bernevig, and Q. Wu, Moiré fractional chern insulators. i. first-principles calculations and continuum models of twisted bilayer mote₂, *Phys. Rev. B* **109**, 205121 (2024).
- [62] J. Herzog-Arbeitman, Y. Wang, J. Liu, P. M. Tam, Z. Qi, Y. Jia, D. K. Efetov, O. Vafek, N. Regnault, H. Weng, Q. Wu, B. A. Bernevig, and J. Yu, Moiré fractional chern insulators. ii. first-principles calculations and continuum models of rhombohedral graphene superlattices, *Phys. Rev. B* **109**, 205122 (2024).
- [63] Y. H. Kwan, J. Yu, J. Herzog-Arbeitman, D. K. Efetov, N. Regnault, and B. A. Bernevig, Moiré fractional chern insulators iii: Hartree-fock phase diagram, magic angle regime for chern insulator states, the role of the moiré potential and goldstone gaps in rhombohedral graphene superlattices (2023), arXiv:2312.11617 [cond-mat.str-el].
- [64] J. Yu, J. Herzog-Arbeitman, Y. H. Kwan, N. Regnault, and B. A. Bernevig, Moiré fractional chern insulators iv: Fluctuation-driven collapse of fcis in multi-band exact diagonalization calculations on rhombohedral graphene (2024), arXiv:2407.13770 [cond-mat.str-el].
- [65] D. Waters, A. Okounkova, R. Su, B. Zhou, J. Yao, K. Watanabe, T. Taniguchi, X. Xu, Y.-H. Zhang, J. Folk, and M. Yankowitz, Interplay of electronic crystals with integer and fractional chern insulators in moiré pentalayer graphene (2024), arXiv:2408.10133 [cond-mat.mes-hall].
- [66] Y.-H. Zhang, Vortex spin liquid with fractional quantum spin hall effect in moiré chern bands (2024), arXiv:2402.05112 [cond-mat.str-el].
- [67] V. Kalmeyer and R. B. Laughlin, Equivalence of the resonating-valence-bond and fractional quantum hall states, *Phys. Rev. Lett.* **59**, 2095 (1987).
- [68] V. Kalmeyer and R. B. Laughlin, Theory of the spin liquid state of the heisenberg antiferromagnet, *Phys. Rev. B* **39**, 11879 (1989).
- [69] L. Savary and L. Balents, Quantum spin liquids: a review, *Reports on Progress in Physics* **80**, 016502 (2016).
- [70] Y. Zhou, K. Kanoda, and T.-K. Ng, Quantum spin liquid states, *Reviews of Modern Physics* **89**, 025003 (2017).
- [71] Y.-Q. Wang, C. Liu, and J. E. Moore, Structure of domain walls in chiral spin liquids (2022), arXiv:2208.14056 [cond-mat.str-el].
- [72] A. Kitaev, Anyons in an exactly solved model and beyond, *Annals of Physics* **321**, 2 (2006).
- [73] H. Yao and S. A. Kivelson, Exact chiral spin liquid with non-abelian anyons, *Phys. Rev. Lett.* **99**, 247203 (2007).
- [74] H. Yao and D.-H. Lee, Fermionic magnons, non-abelian spinons, and the spin quantum hall effect from an exactly solvable spin-1/2 kitaev model with su(2) symmetry, *Phys. Rev. Lett.* **107**, 087205 (2011).
- [75] A. Szasz, J. Motruk, M. P. Zaletel, and J. E. Moore, Chiral spin liquid phase of the triangular lattice hubbard model: a density matrix renormalization group study, *Physical Review X* **10**, 021042 (2020).
- [76] D. T. Son, Is the composite fermion a dirac particle?, *Phys. Rev. X* **5**, 031027 (2015).

- [77] G. Moore and N. Read, Nonabelions in the fractional quantum hall effect, *Nuclear Physics B* **360**, 362 (1991).
- [78] T. Tan and T. Devakul, Parent berry curvature and the ideal anomalous hall crystal, arXiv preprint arXiv:2403.04196 (2024).
- [79] Note that, this form of electron-phonon interaction asymptotically approaches the delta function as $q_0 \rightarrow 0$. See Ref. [94] for further details.
- [80] J. Shi and Q. Niu, Attractive electron-electron interaction induced by geometric phase in a bloch band, arXiv preprint cond-mat/0601531 (2006).
- [81] In numerical calculations we find the superconducting phase is relatively inert to d , but rather sensitive to q_0 which is consistent with Ref. [80]. When q_0 is enlarged, the area of BEC phase grows, while the area of TSC phase shrinks. This suggests that a more extended electron-phonon coupling will favor superconductivity but suppress topological physics.
- [82] For the C_3 symmetric system, the p -wave and the d -wave superconductors are related by a time reversal transformation, since the former one has angular momentum $l = +1$ and the latter has $l = +2 = -1 \pmod{3}$.
- [83] Y. Li and F. D. M. Haldane, Topological nodal cooper pairing in doped weyl metals, *Phys. Rev. Lett.* **120**, 067003 (2018).
- [84] F. Simon, M. Gabay, M. O. Goerbig, and L. Pagot, Role of the berry curvature on bcs-type superconductivity in two-dimensional materials, *Phys. Rev. B* **106**, 214512 (2022).
- [85] V. Crépel, D. Guerci, J. Cano, J. H. Pixley, and A. Millis, Topological superconductivity in doped magnetic moiré semiconductors, *Phys. Rev. Lett.* **131**, 056001 (2023).
- [86] N. Seiberg, T. Senthil, C. Wang, and E. Witten, A duality web in 2+1 dimensions and condensed matter physics, *Annals of Physics* **374**, 395 (2016).
- [87] T. Senthil, D. T. Son, C. Wang, and C. Xu, Duality between (2+1)d quantum critical points, *Physics Reports* **827**, 1 (2019), duality between (2+1)d quantum critical points.
- [88] D. S. Antonenko, L. Fu, and L. I. Glazman, Making s-wave superconductors topological with magnetic field (2024), arXiv:2409.15266 [cond-mat.supr-con].
- [89] X.-G. Wen, Topological orders and edge excitations in fractional quantum hall states, in *Field Theory, Topology and Condensed Matter Physics* (Springer Berlin Heidelberg, Berlin, Heidelberg, 1995) pp. 155–176.
- [90] L. Fu and C. L. Kane, Superconducting proximity effect and majorana fermions at the surface of a topological insulator, *Phys. Rev. Lett.* **100**, 096407 (2008).
- [91] Integrating out Majorana fermion will generate a gravitational CS term [76], which is not the focus of our study here and omitted in the field theory Eq. (11). Self CS term of the \mathbb{Z}_2 gauge field is not generated since Majorana fermion does not suffer the parity anomaly.
- [92] T. H. Hansson, A. Karlhede, and M. Sato, Topological field theory for p-wave superconductors, *New Journal of Physics* **14**, 063017 (2012).
- [93] E. Fradkin and S. H. Shenker, Phase diagrams of lattice gauge theories with higgs fields, *Physical Review D* **19**, 3682 (1979).
- [94] M. M. Parish, The bcs-bec crossover, in *Quantum Gas Experiments* (World Scientific, 2014) Chap. Chapter 9, pp. 179–197

SUPPLEMENTARY MATERIAL

I. HATREE-FOCK CALCULATION FOR INSULATING PHASE

For the insulating phase we decompose the electron momentum as $(\mathbf{k} + \mathbf{g})$, where \mathbf{k} is defined in the first BZ, and \mathbf{g} labels the reciprocal lattice vectors. Under this notation the Hamiltonian reads

$$H_0 = \sum_{\mathbf{k} \in \text{BZ}} \sum_{\mathbf{g}} \epsilon(\mathbf{k} + \mathbf{g}) c_{\mathbf{k}+\mathbf{g}}^\dagger c_{\mathbf{k}+\mathbf{g}}, \quad (\text{S1})$$

and

$$H_{\text{int}} = \sum_{\mathbf{k} \in \text{BZ}} \sum_{\mathbf{g}_1, \mathbf{g}_2, \mathbf{g}_3, \mathbf{g}_4} S(\mathbf{k}_1 + \mathbf{g}_1 - \mathbf{k}_4 - \mathbf{g}_4) \mathcal{F}_{\mathbf{k}_1 + \mathbf{g}_1, \mathbf{k}_4 + \mathbf{g}_4} \mathcal{F}_{\mathbf{k}_2 + \mathbf{g}_2, \mathbf{k}_3 + \mathbf{g}_3} c_{\mathbf{k}_1 + \mathbf{g}_1}^\dagger c_{\mathbf{k}_2 + \mathbf{g}_2}^\dagger c_{\mathbf{k}_3 + \mathbf{g}_3} c_{\mathbf{k}_4 + \mathbf{g}_4} \\ \times \delta_{\mathbf{k}_1 + \mathbf{g}_1 + \mathbf{k}_2 + \mathbf{g}_2 - \mathbf{k}_3 - \mathbf{g}_3 - \mathbf{k}_4 - \mathbf{g}_4}. \quad (\text{S2})$$

Under the Hartree-Fock approximation, the interaction Hamiltonian can be decomposed into the Hartree term with $\mathbf{k}_1 = \mathbf{k}_4$ and $\mathbf{k}_2 = \mathbf{k}_3$:

$$H_{\text{H}} = E_{\text{H}} + \sum_{\mathbf{k} \in \text{BZ}} \sum_{\mathbf{g}_1, \mathbf{g}_2, \mathbf{g}_3, \mathbf{g}_4} 2S(\mathbf{g}_1 - \mathbf{g}_4) \mathcal{F}_{\mathbf{k}_1 + \mathbf{g}_1, \mathbf{k}_1 + \mathbf{g}_4} \mathcal{F}_{\mathbf{k}_2 + \mathbf{g}_2, \mathbf{k}_2 + \mathbf{g}_3} P_{\mathbf{g}_1, \mathbf{g}_4}(\mathbf{k}_1) c_{\mathbf{k}_2 + \mathbf{g}_2}^\dagger c_{\mathbf{k}_2 + \mathbf{g}_3} \\ \times \delta_{\mathbf{g}_1 + \mathbf{g}_2 - \mathbf{g}_3 - \mathbf{g}_4}, \quad (\text{S3})$$

and the Fock term with $\mathbf{k}_1 = \mathbf{k}_3$ and $\mathbf{k}_2 = \mathbf{k}_4$:

$$H_{\text{F}} = E_{\text{F}} - \sum_{\mathbf{k} \in \text{BZ}} \sum_{\mathbf{g}_1, \mathbf{g}_2, \mathbf{g}_3, \mathbf{g}_4} 2S(\mathbf{k}_1 + \mathbf{g}_1 - \mathbf{k}_2 - \mathbf{g}_4) \mathcal{F}_{\mathbf{k}_1 + \mathbf{g}_1, \mathbf{k}_2 + \mathbf{g}_4} \mathcal{F}_{\mathbf{k}_2 + \mathbf{g}_2, \mathbf{k}_1 + \mathbf{g}_3} P_{\mathbf{g}_1, \mathbf{g}_3}(\mathbf{k}_1) c_{\mathbf{k}_2 + \mathbf{g}_2}^\dagger c_{\mathbf{k}_2 + \mathbf{g}_4} \\ \times \delta_{\mathbf{g}_1 + \mathbf{g}_2 - \mathbf{g}_3 - \mathbf{g}_4}. \quad (\text{S4})$$

Here

$$P_{\mathbf{g}_i, \mathbf{g}_j}(\mathbf{k}) = \left\langle c_{\mathbf{k} + \mathbf{g}_i}^\dagger c_{\mathbf{k} + \mathbf{g}_j} \right\rangle \quad (\text{S5})$$

is the mean-field ansatz. The constant energy shift $E_{\text{H/F}}$ reads

$$E_{\text{H}} = - \sum_{\mathbf{k} \in \text{BZ}} \sum_{\mathbf{g}_1, \mathbf{g}_2, \mathbf{g}_3, \mathbf{g}_4} S(\mathbf{g}_1 - \mathbf{g}_4) \mathcal{F}_{\mathbf{k}_1 + \mathbf{g}_1, \mathbf{k}_1 + \mathbf{g}_4} \mathcal{F}_{\mathbf{k}_2 + \mathbf{g}_2, \mathbf{k}_2 + \mathbf{g}_3} P_{\mathbf{g}_1, \mathbf{g}_4}(\mathbf{k}_1) P_{\mathbf{g}_2, \mathbf{g}_3}(\mathbf{k}_2) \delta_{\mathbf{g}_1 + \mathbf{g}_2 - \mathbf{g}_3 - \mathbf{g}_4}, \quad (\text{S6})$$

$$E_{\text{F}} = \sum_{\mathbf{k} \in \text{BZ}} \sum_{\mathbf{g}_1, \mathbf{g}_2, \mathbf{g}_3, \mathbf{g}_4} S(\mathbf{k}_1 + \mathbf{g}_1 - \mathbf{k}_2 - \mathbf{g}_4) \mathcal{F}_{\mathbf{k}_1 + \mathbf{g}_1, \mathbf{k}_2 + \mathbf{g}_4} \mathcal{F}_{\mathbf{k}_2 + \mathbf{g}_2, \mathbf{k}_1 + \mathbf{g}_3} P_{\mathbf{g}_1, \mathbf{g}_3}(\mathbf{k}_1) P_{\mathbf{g}_2, \mathbf{g}_4}(\mathbf{k}_2) \delta_{\mathbf{g}_1 + \mathbf{g}_2 - \mathbf{g}_3 - \mathbf{g}_4}. \quad (\text{S7})$$

In calculation we choose total 7 BZs with the first BZ centered and the other 6 BZs packed around it, and 108 \mathbf{k} points within each BZ. The electron filling is set to be $\nu = 1$, which means the total number of electron N is equal to the number of \mathbf{k} points in the first BZ, i.e. $N = 108$. The ground state energy of the insulating phase under the Hartree-Fock approximation is

$$E_{\text{HF}} = \sum_{\mathbf{k} \in \text{BZ}} \langle \mathbf{k} | H_0 + H_{\text{H}} + H_{\text{F}} | \mathbf{k} \rangle = -E_{\text{H}} - E_{\text{F}} + \sum_{\mathbf{k} \in \text{BZ}} \epsilon(\mathbf{k}). \quad (\text{S8})$$

II. MEAN-FIELD CALCULATION FOR SUPERCONDUCTING PHASE

For the superconducting phase we assume the pairing happens between electrons with opposite momenta. The mean-field interaction Hamiltonian reads

$$H_{\text{SC}} = \sum_{\mathbf{k}, \mathbf{k}'} S(\mathbf{k} - \mathbf{k}') \mathcal{F}_{\mathbf{k}, \mathbf{k}'}^2 c_{\mathbf{k}}^\dagger c_{-\mathbf{k}}^\dagger \langle c_{-\mathbf{k}'} c_{\mathbf{k}'} \rangle + h.c. \quad (\text{S9})$$

Define the superconducting gap

$$\Delta(\mathbf{k}) = \sum_{\mathbf{k}'} \frac{1}{2} [S(\mathbf{k} - \mathbf{k}') \mathcal{F}_{\mathbf{k}, \mathbf{k}'}^2 - S(-\mathbf{k} - \mathbf{k}') \mathcal{F}_{-\mathbf{k}, \mathbf{k}'}^2] \langle c_{-\mathbf{k}'} c_{\mathbf{k}'} \rangle, \quad (\text{S10})$$

which respects spatial asymmetry $\Delta(-\mathbf{k}) = -\Delta(\mathbf{k})$ for the pairing of spinless fermion. Then the BdG Hamiltonian reads

$$H_{\text{BdG}} = \sum_{\mathbf{k}} \Psi_{\mathbf{k}}^\dagger \begin{pmatrix} [\epsilon(\mathbf{k}) - \mu]/2 & \Delta(\mathbf{k}) \\ \Delta^*(\mathbf{k}) & [-\epsilon(\mathbf{k}) + \mu]/2 \end{pmatrix} \Psi_{\mathbf{k}}, \quad (\text{S11})$$

where $\Psi_{\mathbf{k}} = (c_{\mathbf{k}}, c_{-\mathbf{k}}^\dagger)^\text{T}$ is the Nambu spinor, and μ is the chemical potential. The self-consistent equations for the gap $\Delta(\mathbf{k})$ and the chemical potential μ read

$$\Delta(\mathbf{k}) = - \sum_{\mathbf{k}'} \frac{\Delta(\mathbf{k}')}{4E(\mathbf{k}')} [S(\mathbf{k} - \mathbf{k}') \mathcal{F}_{\mathbf{k}, \mathbf{k}'}^2 - S(\mathbf{k} + \mathbf{k}') \mathcal{F}_{-\mathbf{k}, \mathbf{k}'}^2], \quad (\text{S12})$$

$$N = \sum_{\mathbf{k}} 1 - \frac{\epsilon(\mathbf{k})}{E(\mathbf{k})}, \quad (\text{S13})$$

where $E(\mathbf{k}) = \sqrt{[\epsilon(\mathbf{k}) - \mu]^2/4 + |\Delta(\mathbf{k})|^2}$ is the dispersion of the Bogoliubov band, which depends on μ implicitly. $N = 108$ is the total number of electrons introduced in the previous section. The total energy of the superconducting state is

$$E_{\text{SC}} = \sum_{\mathbf{k}} \frac{\epsilon(\mathbf{k}) - \mu}{2} - E(\mathbf{k}) + \frac{|\Delta(\mathbf{k})|^2}{2E(\mathbf{k})}. \quad (\text{S14})$$

In numerics we check the convergence of particle-particle and particle-hole channels for each pair of (u, v) , and if both channels converge the energetic favored one is picked.

Note that the electron-phonon coupling potential we adopt, $U(\mathbf{q}) = q_0^2/(|\mathbf{q}|^2 + q_0^2)$, interpolates between the BCS limit and the case for real materials as q_0 varies. Here we would like to show that the phase diagram is qualitatively insensitive to the details of the electron-phonon coupling potential. For $q_0 \gg |\mathbf{K}|$, $U(\mathbf{q})$ becomes nearly uniform, which is close to the BCS limit. On the contrary, when $q_0 \ll |\mathbf{K}|$, $U(\mathbf{q})$ asymptotes a delta function, which better describes materials. To see the variation of q_0 does not eliminate the chiral topological superconductor phase, we calculate the phase diagrams shown in Fig. [S1 (a-c)] with (a) $q_0 = 0.05|\mathbf{K}|$, (b) $q_0 = 0.3|\mathbf{K}|$ (the same as that in the main text), and (c) $q_0 = 20|\mathbf{K}|$. It can be seen that chiral topological superconductivity indeed does not vanish, though disfavored by both large and small q_0 . For large q_0 , the uniformness of $U(\mathbf{q})$ effectively leads to an enhanced coupling strength of the attractive interaction, which favors a trivial gapped BEC phase. On the other hand, for small q_0 , since $U(\mathbf{q})$ is close to a delta function, the Berry curvature effect, relying on a finite \mathbf{q} and crucial to the formation of TSC, will be suppressed. If $q_0 = 0$, the superconductivity arises solely from Cooper instability, and the Berry curvature effect is completely screened. In this case the superconducting phase should be a nodal p -wave superconductor, instead of a gapped chiral topological one.

III. K -MATRIX CALCULATION AND NON-ABELIAN STATISTICS IN FIELD THEORY

As stated in the main text, in the non-superconducting phases of the composite fermion, the topological part of the Lagrangian reads

$$\mathcal{L}_{\text{QH}} = -\Theta(-m) \frac{i}{4\pi} a da - \frac{i}{2\pi} a db - \frac{2i}{4\pi} b db - \frac{i}{2\pi} b dA. \quad (\text{S15})$$

Its corresponding K -matrix reads

$$K_{\text{QH}} = \begin{pmatrix} \Theta(-m) & 1 \\ 1 & 2 \end{pmatrix}, \quad (\text{S16})$$

which does not host topological order since $|\det K| = 1$. The charge vector is $\mathbf{p} = (0, 1)^\text{T}$, and hence the Hall conductance is $\sigma_H = \mathbf{p}^\text{T} K_{\text{QH}}^{-1} \mathbf{p} = -\Theta(-m)$. Thus $\sigma_H = 0$ for $m > 0$ and $\sigma_H = 1$ for $m < 0$. A topological phase transition occurs at $m = 0$, where the composite fermion is gapless.

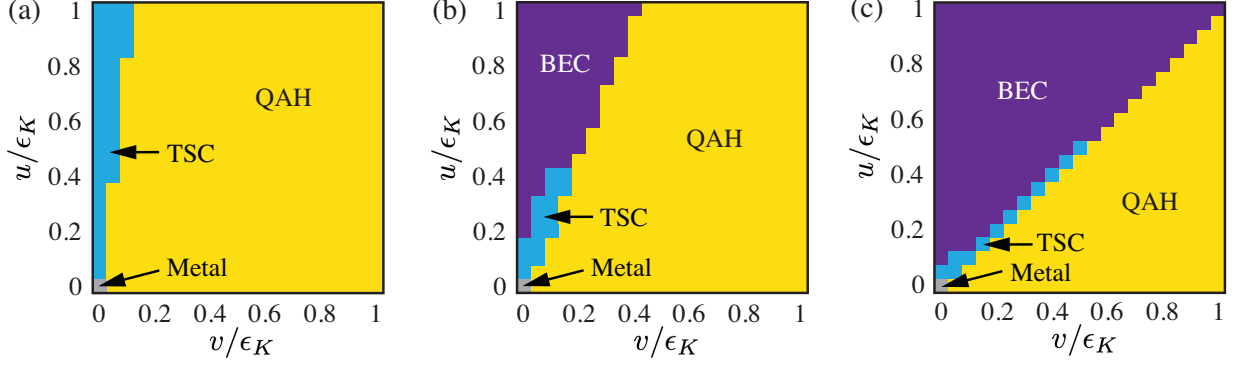


FIG. S1. The phase diagrams for (a) $q_0 = 0.05|\mathbf{K}|$, (b) $q_0 = 0.3|\mathbf{K}|$, and (c) $q_0 = 20|\mathbf{K}|$. As q_0 increases, the area of the trivial gapped BEC phase is enlarged, while the area of the TSC phase is reduced. When $q_0 \ll |\mathbf{K}|$, as the case of (a), in the TSC regime the energies of $(p+ip)$ -wave and $(p-ip)$ -wave superconducting states become nearly degenerate, and the self-consistent calculations are difficult to converge. These implies a possible nodal p -wave superconducting phase instead of a gapped TSC phase.

In the Moore-Read phase, the effective Lagrangian capturing the Abelian part of the anyon statistics is

$$\mathcal{L}_{\text{MR}} = \frac{1}{2\kappa}(da)^2 + \frac{2i}{2\pi}ad\tilde{a} - \frac{i}{2\pi}adb - \frac{2i}{4\pi}bdb - \frac{i}{2\pi}bdA. \quad (\text{S17})$$

Its corresponding K -matrix is

$$K_{\text{MR}} = \begin{pmatrix} 0 & -2 & 1 \\ -2 & 0 & 0 \\ 1 & 0 & 2 \end{pmatrix} \quad (\text{S18})$$

with charge vector $\mathbf{q} = (0, 0, 1)^{\text{T}}$. The Hall conductance in this phase $\sigma_H = \mathbf{q}^{\text{T}}K_{\text{MR}}^{-1}\mathbf{q} = 1/2$. The vortex carrying “magnetic charge” under the \mathbb{Z}_2 gauge field a has its current coupled to \tilde{a} . Thus, its l -vector is $\mathbf{l}_v = (0, 1, 0)$. The vortex carries charge $Q_v = \mathbf{l}_v^{\text{T}}K_{\text{MR}}^{-1}\mathbf{q} = 1/4$ and self-statistical angle $\theta_v = \pi\mathbf{l}_v^{\text{T}}K_{\text{MR}}^{-1}\mathbf{l}_v = \pi/8$. The quasi hole whose current is coupled to gauge field c has $\mathbf{l}_h = (0, 0, 1)$. Therefore it has half charge $Q_h = \mathbf{l}_h^{\text{T}}K_{\text{MR}}^{-1}\mathbf{q} = 1/2$ and semionic self-statistics $\theta_h = \pi\mathbf{l}_h^{\text{T}}K_{\text{MR}}^{-1}\mathbf{l}_h = \pi/2$. The incorporation of Majorana zero modes reads

$$\mathcal{L}_{\text{Majorana}} = \frac{2i}{2\pi} \left(\tilde{a} + \frac{1}{4}\eta id\eta \right) da - i\tilde{a}_\mu j_\mu^v - ib_\mu j_\mu^h - \frac{i}{2\pi}adb - \frac{2i}{4\pi}bdb - \frac{i}{2\pi}bdA, \quad (\text{S19})$$

where j_μ^v and j_μ^h are the currents of the vortices and the quasi holes, respectively, while the Majorana zero modes are described by η . Equations of motion for \tilde{a} and b gives rise to

$$j_\mu^v = \frac{1}{\pi}\epsilon_{\mu\nu\lambda}\partial_\nu a_\lambda, \quad j_\mu^h = -\frac{1}{2\pi}\epsilon_{\mu\nu\lambda}\partial_\nu(2b_\lambda + a_\lambda + A_\lambda). \quad (\text{S20})$$

Accordingly, the Majorana theory Eq. (S19) can be formally written as

$$\mathcal{L}_{\text{Majorana}} = \frac{1}{4}j_\mu^v \eta i \partial_\mu \eta + \frac{\pi}{8}j_\nu^v \frac{i}{\partial} j_\nu^v + \frac{1}{4}iA_\mu j_\mu^v + \frac{\pi}{2}j_\nu^v \frac{i}{\partial} j_\nu^h + \frac{\pi}{2}j_\nu^h \frac{i}{\partial} j_\nu^h + \frac{1}{2}iA_\mu j_\mu^h, \quad (\text{S21})$$

after integrating out all the dynamical gauge fields. Here $1/\partial$ is a shorthand of the current-current interaction mediated by gauge fields. The first term describing vortices trapping Majorana zero modes gives rise to the desired non-Abelian statistics. The charge and the Abelian self-statistical angle of vortices, $Q_v = 1/4$ and $\theta_v = \pi/8$ respectively, can also be manifestly read off, and similarly for the quasi holes.